

Quasiparticle generation efficiency in superconducting thin-films

T. Guruswamy, D. J. Goldie and S. Withington
*Detector and Optical Physics Group,
 Cavendish Laboratory, University of Cambridge,
 J J Thomson Avenue, Cambridge, CB3 0HE, UK*
 *

(Dated: January 10, 2014)

Thin-film superconductors with thickness $\sim 30 - 500$ nm are used as non-equilibrium quantum detectors for photons, phonons or more exotic particles. One of the most basic questions in determining their limiting sensitivity is the efficiency with which the quanta of interest couple to the detected quasiparticles. As low temperature superconducting resonators, thin-films are attractive candidates for producing quantum-sensitive arrayable sensors and the readout uses an additional microwave probe. We have calculated the quasiparticle generation efficiency η_s for low energy photons in a representative, clean thin-film superconductor (Al) operating well-below its superconducting transition temperature as a function of film thickness, within the framework of the coupled kinetic equations described by Chang and Scalapino.[J. J. Chang and D. J. Scalapino, J. Low Temp. Phys. **31**, 1 (1978)]. We have also included the effect of a lower frequency probe. We show that phonon loss from the thin-film reduces η_s by as much as 40% compared to earlier models that considered relatively thick films or infinite volumes. We also show that the presence of the probe and signal *enhances* the generation efficiency slightly. We conclude that the ultimate limiting noise equivalent power of this class of detector is determined by the thin-film geometry.

PACS numbers: 74.40.Gh, 74.78.-w, 29.40.-n, 74.25.N-
 Keywords:

I. INTRODUCTION

Superconductive detectors have revolutionized experimental astrophysics. Many of these detectors exploit Cooper pair-breaking in a thin-film low transition temperature superconductor operating at low reduced temperatures $T/T_c \simeq 0.1$ (T is the temperature and T_c is the superconducting transition temperature, $T_c \sim 1$ K). These detectors rely on non-equilibrium effects but to our knowledge no detailed microscopic description exists of the efficiency with which the excess quasiparticles are created in a thin-film superconductor of thickness $\sim 30 - 500$ nm. This problem is very relevant not just for kinetic inductance detectors (KIDs),^{1,2} but also for superconducting tunnel junction detectors,³ single photon counting nanowires,⁴ and quantum capacitance detectors.⁵ All of these devices can be fabricated by photolithography usually on a relatively thick substrate such as Si or sapphire that is held at T and that functions as a heat bath. KIDs are thin-film superconducting resonators that can be configured as ultra-sensitive detectors of signal photons across the electromagnetic spectrum. KIDs are typically readout with a microwave probe with photons of energy $h\nu_p \sim 0.05\Delta$, where ν_p is the probe frequency, 2Δ is the low temperature superconducting energy gap and h is Planck's constant. In this instance understanding combined effects of the signal and the probe is clearly important. In Ref. 6 we described a detailed microscopic calculation of the spectrum of the non-equilibrium quasiparticles and phonons in a superconducting resonator operating at $T/T_c = 0.1$ considering only a probe. Ref. 7 compared that model with precise experimental measurements of the temper-

ature and power dependence of the behavior of ultra-sensitive Al resonators, finding good agreement between model and measurement.

In a superconductor each absorbed signal photon with energy $h\nu_s \geq 2\Delta$ breaks a pair (ν_s is the signal frequency). Probably the most important consideration in calculating the detection sensitivity of these photons in *any* thin-film superconducting detector is η_s the average fraction of the photon energy that creates low energy quasiparticles $E \sim \Delta$ where E is the quasiparticle energy. We distinguish the *primary* spectrum of quasiparticles generated by the signal from the driven *quasistatic* population that is established as the primary spectrum relaxes temporally and energetically. Absorbed photons create a spectrum of excess primary quasiparticles that relaxes to energies $E \sim \Delta$ by emitting phonons on a timescale $\tau_{\text{cascade}} \sim 0.1 - 10$ ns,^{8,9} determined by the quasiparticle-phonon scattering time at $E = 3\Delta$. τ_{cascade} is much shorter than the effective loss time from the film of the excess energy contained in the quasistatic distribution by 2Δ -phonon loss. This time is determined by the effective quasiparticle recombination time of the excess τ_r^{eff} provided other relatively slow direct quasiparticle loss-mechanisms such as out-diffusion or tunneling can be ignored. For $T/T_c \sim 0.1$ and for low detected power, $\tau_r^{\text{eff}} \sim \text{ms}$ even in a thin Al film.⁷ Since $\tau_r^{\text{eff}} \gg \tau_{\text{cascade}}$ the low energy quasistatic population determines the detector response. During the energy relaxation pair-breaking by the emitted phonons occurs provided $\Omega \geq 2\Delta$ (Ω is the phonon energy) and this increases the quasistatic population near Δ , although phonon loss is also possible with characteristic time τ_l . At low temperature and low phonon energies $\Omega \sim 2\Delta$, the pair-

breaking time $\tau_{pb}(\Omega) \sim \tau_0^\phi$ where τ_0^ϕ is the characteristic phonon lifetime.¹⁰ We assume that τ_l is independent of Ω and is determined by the film thickness and the coupling to the substrate.¹¹ For thin-films τ_l is comparable with, or even less than τ_{pb} . Phonon-loss means that energy is lost from any finite thickness film before the quasistatic population is established.

Up to this point we have ignored the effect of the electron-electron interaction in the energy down-conversion. Figure 1 shows the energy dependence of the *normal-state* scattering rates due to the electron-phonon (e- ϕ) interaction $\tau_{e\phi}^{-1}$,¹⁰ the clean-limit electron-electron (e-e) rate τ_{ee}^{-1} which is also valid for disordered films at high energies,^{8,12} and the e-e rate including the effect of disorder $(\tau_{ee}(D))^{-1}$,^{13,14} where D denotes the diffusion coefficient. The calculations assume an Al thickness $d = 35$ nm with resistivity $\rho = 8 \times 10^{-8}$ Ωm , typical of a clean Al film on Al_2O_3 ,⁷ that is representative of the thinnest films modeled here. For $E > 200\Delta$, $(\tau_{e\phi})^{-1}$ is cut-off at the Debye energy Ω_D . At the highest energies $E \sim 10^4\Delta$ e-e scattering becomes the main energy relaxation mechanism. At lower energies ($E \sim 25\Delta$) disorder increases the e-e rate in this instance. For $E \sim 1.2\Delta$ we see that the e-e and e- ϕ rates again become equal. For $1.2\Delta < E < 10^4\Delta$ the e- ϕ interaction is the principal relaxation mechanism. A detailed description of the energy dependence of the disorder-enhanced e-e rate in a superconductor at low T/T_c , including the effect of the energy gap, seems to be lacking although for $E = \Delta$ the e-e rate is further reduced compared to e- ϕ becoming negligible.¹⁵ We note also that the energy scale of interest determining the relative importance of low energy e-e compared to e- ϕ scattering in the relaxation is not Δ but rather 3Δ : below this energy pair-breaking is forbidden for both. For the thicker Al films discussed below D is enhanced in clean films so that the effect of disorder is again reduced. For these reasons we ignore e-e relaxation for all energy scales, temperatures and film parameters considered. Extrapolation of our results to other low- T_c superconductors should thus be done with caution particularly for higher resistivity or very thin films.

A number of calculations exist of η_s for high energy photons $h\nu_s \gg 2\Delta$ and Ω_D that have considered infinite superconducting volumes finding $\eta_s \sim 0.57$ – 0.6 for Al,⁸ Nb¹⁶ and Sn.¹⁷ Hijmering *et al.*¹⁸ calculated quasiparticle creation efficiencies in thin-film Al-Ta bilayers taking account of the modification of the quasiparticle density of states due to the proximity effect but ignored loss of pair-breaking phonons. Zehnder¹⁹ calculated η_s in a number of thin film superconductors with thickness $d = 500$ nm at $T = 0.5$ K including quasiparticle diffusion and phonon loss. η_s was determined from the number of quasiparticles remaining at time $t \simeq 10$ ns when the initial energy down-conversion was considered complete giving $\eta_s \sim 0.7$ for Al.

Here we consider the regime $90 \leq \nu_s \leq 450$ GHz. To date no work has calculated η_s for these signal photon energies at low T/T_c , or the technologically impor-

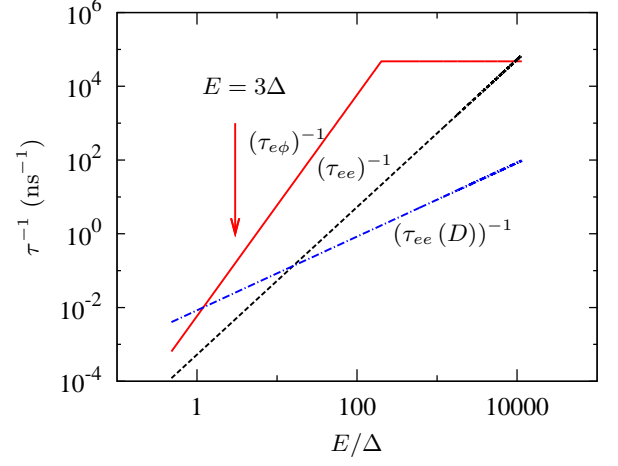


FIG. 1: (Color online) Energy dependence of the relaxation rates in a clean, thin Al film in the normal state: (red) solid line electron-phonon scattering, (black) dashed line clean-limit electron-electron scattering and (blue) dash-dot line the electron-electron scattering time including the effect of disorder. The calculations are for a 35 nm Al film with $\rho = 8 \times 10^{-8}$ Ωm . Δ is the low temperature energy gap.

tant range of film thicknesses considered here including 2Δ -phonon loss. This frequency range is particularly relevant for mm- and sub-mm astronomy. We have also included a lower frequency probe. We followed Chang and Scalapino²⁰ to solve the coupled kinetic equations describing the quasiparticle and phonon populations. Our approach explicitly includes the contribution of all phonon branches because it relies on the measured Eliashberg function $\alpha^2 F(\Omega)$ in the calculation of the characteristic times¹⁰ and the sum over the three branches is essential to conserve energy.⁶

II. THE EFFECT OF A PAIR-BREAKING SIGNAL

The coupled kinetic equations described in Ref. 20 were solved using Newton-Raphson iteration to find the non-equilibrium quasiparticle and phonon energy distributions $f(E)$ and $n(\Omega)$. Details of the scheme are given in Ref. 6. The absorbed powers per unit volume from the signal P_s and probe P_p are assumed to be spatially uniform. We ignore changes in Δ due to P_s and P_p . In Ref. 7 we found that changes in Δ were very small $\ll 0.001\Delta$ for typical experimental P_p . The effect of P_s is to introduce an additional drive term²¹ into Eq. [2] of Ref. 6 for the quasiparticle distribution function $\delta f(E)/\delta t|_s = I_s$ where $I_s = B_s K_s$,

$$K_s(E, \nu_s) = K_p(E, \nu_s) + 2\rho(E', \Delta) \left[1 - \frac{\Delta^2}{EE'} \right] \times [1 - f(E) - f(E')], \quad (1)$$

$E' = h\nu_s - E$ and the prefactor B_s is calculated with $B_s = P_s/4N(0) \int_{\Delta}^{\infty} E\rho(E)K_s(E, \nu_s)dE$, ensuring that the absorption of P_s conserves energy. A prefactor for the probe power absorption B_p can be similarly defined.⁶ $N(0)$ is the single-spin electronic density of states. Some solutions require calculation of differences between distributions. To ensure numerical accuracy we increased the precision requirements in the code so that the errors in the power flow between the quasiparticles and thin-film phonons and then the heat bath phonons (see Ref. 6 for details) were converged to better than 2×10^{-6} and likewise the iterated solutions for B_s and B_p . We used a quasiparticle density of states $\rho(E, \Delta) = \text{Re} \left((E + i\gamma) / ((E + i\gamma)^2 - \Delta^2)^{1/2} \right)$. The factor γ takes account of the broadening of the peak in ρ near $E = \Delta$ due to lifetime effects or film inhomogeneity.¹ The choice $\gamma = 1.125 \times 10^{-3}\Delta$ minimizes the difference between the thermal quasiparticle number density N_T calculated by summing over the discretized distributions (where we used a $1 \mu\text{eV}$ grid) compared to numerical integration of the functions $N_T = 4N(0) \int_{\Delta}^{\infty} \rho(E, \Delta)f(E, T)dE$ where $f(E, T) = 1/(1 + \exp(E/k_bT))$ is the Fermi-Dirac function and k_b is Boltzmann's constant. We used parameters of a thin Al film as in Ref. 6: $\Delta = 180 \mu\text{eV}$, $T_c = 1.17 \text{ K}$, $N(0) = 1.74 \times 10^4 \mu\text{eV}^{-1} \mu\text{m}^{-3}$, characteristic quasiparticle time $\tau_0 = 438 \text{ ns}$.¹⁰ $\tau_0^{\phi} = 0.26 \text{ ns}$ and $T/T_c = 0.1$. This ratio of τ_0/τ_0^{ϕ} means that our numerical solutions conserve energy, they are *not* independent variables: Eq. [11] of Ref. 6 gives the overall parameter dependencies. The value we use for τ_0 has given a good account of the temperature dependence of the generation-recombination noise measured in clean, thin Al films.^{7,22} in which the effect of phonon trapping should be small (we estimate $\tau_l/\tau_0^{\phi} \sim 0.5$ in this case). A number of previous authors have used $\tau_0 \sim 100 \text{ ns}$,²³ although this value seems inconsistent with the more recent measurements. Wilson and Prober have also observed unexpectedly long lifetimes in 200 nm Al films (estimating τ_0 to be even longer than the value used here), and suggested the observation resulted from an anomalously long τ_l .²⁴ Interestingly the longer τ_0 seems to be associated with those measurements that have implemented stringent experimental procedures to minimize the effect of stray light from higher temperature stages in cryogenic systems: note that typical photon energies emitted by a 4 K source significantly exceed 2Δ in Al. Where used we assumed $h\nu_p = 16 \mu\text{eV}$ ($\nu_p = 3.88 \text{ GHz}$).

III. CALCULATING η_s

Consider m , the average number of driven quasistatic quasiparticles generated by each absorbed photon. Signal photons interact with rate $\Gamma_{\Phi} = P_s/h\nu_s$ and each photon creates two primary quasiparticles. These rapidly relax in energy generating the driven quasistatic popu-

lation with rate $\Gamma_s = m\Gamma_{\Phi}$. Assuming that all of the excess quasiparticles have $E = \Delta$ then $\eta_s = m\Delta/h\nu_s = \Gamma_s\Delta/P_s$. We use a modified set of Rothwarf-Taylor rate equations²⁵ to find Γ_s . With Γ_p the generation rate of quasistatic quasiparticles due to the probe, N the number density of quasiparticles and $N_{2\Delta}$ the number density of 2Δ -phonons

$$\frac{dN}{dt} = \Gamma_s + \Gamma_p - RN^2 + 2\beta N_{2\Delta}, \quad (2)$$

$$\frac{dN_{2\Delta}}{dt} = \frac{RN^2}{2} - \beta N_{2\Delta} - \frac{N_{2\Delta} - N_{2\Delta}^T}{\tau_l}. \quad (3)$$

Here R and β are the recombination and pair-breaking coefficients respectively and $N_{2\Delta}^T$ is the thermal density of 2Δ -phonons. We assume that Γ_s and Γ_p are independent. With $\Gamma_s = 0$, Eqs. 2 and 3 can be solved by first also setting $\Gamma_p = 0$ so that in steady-state, $dN/dt = dN_{2\Delta}/dt = 0$, giving $RN_T^2/2 = \beta N_{2\Delta}^T$. This leads to $\Gamma_p = R(N_p^2 - N_T^2)/(\beta\tau_l + 1)$, where N_p is the total number density of quasiparticles with the probe. For the additional signal Γ_s we find

$$\Gamma_s = R(N^2 - N_p^2) \frac{1}{\beta\tau_l + 1}. \quad (4)$$

and with $\beta = 1/\tau_{pb}$

$$\eta_s = \frac{R\Delta(N^2 - N_p^2)}{P_s} \frac{1}{\tau_l/\tau_{pb} + 1}. \quad (5)$$

N and N_p were calculated by numerically integrating solutions of the coupled kinetic equations. We used Eq. (A9) of Chang and Scalapino²⁶ to define a recombination rate R_{CS} . We find that setting $R \equiv 2R_{CS}$ ensures that the population-averaged recombination time $\langle\tau_r\rangle_{qp} = 1/RN$ in thermal equilibrium ($N = N_T$) is the same calculated using either Refs. 26 or 10. We calculate $\langle\tau_{pb}\rangle_{\phi}$ for $f(E)$ and $n(\Omega)$ using Eq. (A10) of Ref. 26. Writing Eq. 4 in terms of the excess number densities N_s^{ex} due to the signal and N_p^{ex} due to the probe alone so that $N = N_s^{ex} + N_p^{ex} + N_T$ and $N_p = N_p^{ex} + N_T$ the effective recombination time $\tau_r^{\text{eff}} = N_s^{ex}/\Gamma_s$ can be calculated for any combination of the magnitudes of N_s^{ex} , N_p^{ex} and N_T . In the calculations reported we consider signal and probe powers relevant to ultra-sensitive KIDs for astronomical applications⁷ so that $N, N_p \gg N_T$ for all cases of P_p, P_s studied.

IV. RESULTS

Fig. 2 shows $f(E)$ for $P_p = 20 \text{ aW}/\mu\text{m}^3$, as the solid curve and the additional effect of $P_s/P_p = 0.01$ (dashed blue curve) with $h\nu_s = 5.1\Delta$. The inset shows the contribution to the number drive $K_s\rho(E, \Delta)$ for the signal normalized so that each absorbed photon produces two

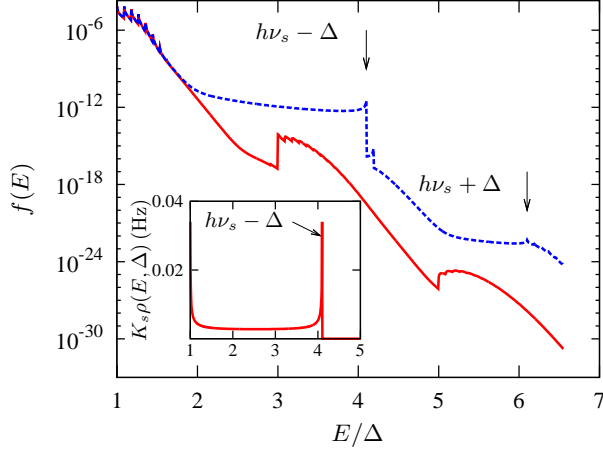


FIG. 2: (Color online) Semi-log plot showing the effect of $P_p = 20 \text{ aW}/\mu\text{m}^3$ on the quasiparticle distribution with $T/T_c = 0.1$: (full red line) probe power only and (dashed blue line) with additional signal $P_s/P_p = 0.01$. The signal photon energy $h\nu_s = 5.1\Delta$ and $\tau_l/\tau_0^\phi = 1$. The inset shows the contribution to the number drive $K_s\rho(E, \Delta)$ for the signal normalized so that each absorbed photon produces two primary quasiparticles per second.

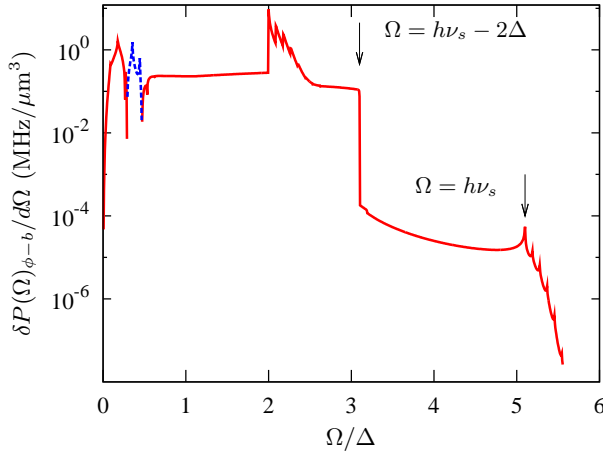


FIG. 3: (Color online) The change in the phonon power flow to the bath $\delta P(\Omega)_{\phi-b}$ for $P_s = 0.01P_p$ and $P_p = 20 \text{ aW}/\mu\text{m}^3$. The signal photon energy $h\nu_s = 5.1\Delta$ and $\tau_l/\tau_0^\phi = 1$. The (blue) dashed section indicates the phonon energies for which the change is negative.

quasiparticles per unit time. The double peak arises because $K_s\rho(E, \Delta)$ involves the *product* of final state densities $\rho(E, \Delta)\rho(E', \Delta)$ which is symmetric with respect to the final state energies. The main figure shows that $f(E)$ for the probe alone has multiply peaked structure at $E \sim \Delta$ due to absorption of the probe photons by the large density of quasiparticles near Δ . At energy $E = 3\Delta$ there is a step in $f(E)$ corresponding to reabsorption of 2Δ -phonons by the driven quasiparticles that also ex-

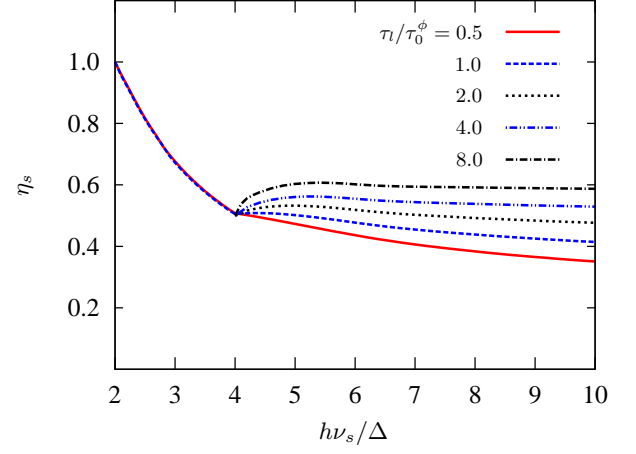


FIG. 4: (Color online) Number generation efficiency η_s as a function of $h\nu_s/\Delta$ for 5 values of τ_l/τ_0^ϕ .

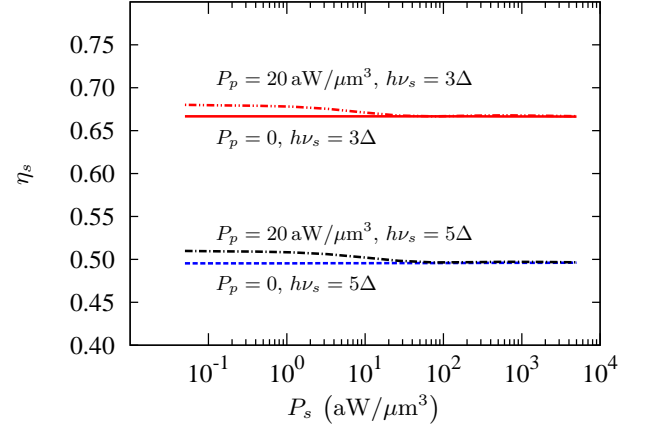


FIG. 5: (Color online) Number generation efficiency η_s for $h\nu_s = 3$ and 5Δ with $P_s = 0$ and $20 \text{ aW}/\mu\text{m}^3$ with $\tau_l/\tau_0^\phi = 1$.

hibits peaks associated with multiple photon absorption from the probe. A smaller feature at $E = 3\Delta - h\nu_p$ is visible that arises from stimulated emission.

The dashed curve showing $f(E)$ with P_s has similar structure at low energies but now shows a step at $E = h\nu_s - \Delta$. The curvature $f(E)$ below this primary peak arises from the energy dependence of the quasiparticle scattering and recombination rates. The peak also has a smaller “satellite” at $E = h\nu_s - \Delta + h\nu_p$ as multiple photon processes involving signal and probe occur. A further similar feature is evident at $E = h\nu_s + \Delta$.

Fig. 3 shows the change in contributions to the power flow to the heat bath $\delta P(\Omega)_{\phi-b} = P(\Omega)_{\phi-b}^s - P(\Omega)_{\phi-b}^p$, where $P(\Omega)_{\phi-b}^s$ is the contribution to the phonon-bath power flow with signal and probe, and $P(\Omega)_{\phi-b}^p$ that for the probe alone. At low phonon energies $\Omega < 0.3\Delta$, $\delta P(\Omega)_{\phi-b}$ is increased due to pair-breaking. At ener-

gies $0.3 < \Omega < 0.5\Delta$ the net flow is negative. The first effect arises as the signal itself has a sharply peaked structure near the gap. The reduction arises from the blocking of final states for the scattering of higher energy probe-generated quasiparticles towards the gap. At higher phonon energies there is a significant change in $\delta P(\Omega)_{\phi-b}$ due to phonons $\Omega \geq 2\Delta$. The spectrum also shows a broad low background contribution at all phonon energies $\Omega \leq (h\nu_s - 2\Delta)$ generated as the primary spectrum scatters to energies $E \sim \Delta$ and at higher Ω from the highest energy quasiparticles shown in Fig. 2.

Fig. 4 shows calculations of η_s as a function of $h\nu_s$ for 5 values of τ_l/τ_0^ϕ . The calculation used $P_s = 0.2 \text{ aW}/\mu\text{m}^3$ and $P_p = 20 \text{ aW}/\mu\text{m}^3$. For $2\Delta \leq h\nu_s \leq 4\Delta$, η_s reduces monotonically and is independent of the phonon loss time. In this regime the high energy primary quasiparticle peak is created at $\Delta \leq E \leq 3\Delta$ and phonons emitted in scattering are unable to break pairs. At higher signal energies $4\Delta \leq h\nu_s \leq 6\Delta$ the efficiency tends to increase again and the increase depends on τ_l/τ_0^ϕ . Pair-breaking enhances η_s and the enhancement depends on the probability of pair-breaking compared to other phonon losses. At higher energies multiple pair-breaking is necessary to create the low energy steady state distribution, but multiple phonon loss also occurs. The overall effect is a reduction in η_s as $h\nu_s$ increases for finite τ_l/τ_0^ϕ . We note that $\eta_s \rightarrow 1$ as $h\nu_s \rightarrow 2\Delta$ for all τ_l/τ_0^ϕ so that Eqs. (2) to (5) and our definition of R self-consistently conserve energy.

Fig. 5 shows η_s for $h\nu_s = 3$ and 5Δ as a function of P_s for two values of the probe power. For $P_p = 0$ the generation efficiency is constant over 5 orders of magnitude of absorbed signal powers. For $P_p = 20 \text{ aW}/\mu\text{m}^3$ and for low signal power, η_s is slightly enhanced. We discuss this in the Sec. V. Fig. 6 shows the distribution-averaged values of τ_r associated with the calculations shown in Fig. 5 (note that Eq. 5 does not involve τ_r explicitly) while Fig. 7 shows τ_{pb} that is directly used in these calculations. Considering Fig. 6 for the small signal regime $P_s \ll P_p$, N_p determines τ_r . For the large signal regime $P_s \gg P_p$, τ_r is independent of P_p because N_s^{ex} determines τ_r . We see that for fixed $h\nu_s$, τ_r changes by nearly three orders of magnitude whilst η_s shown in Fig. 5 is constant for all P_s . (Very close inspection of the results for $P_p = 0$ would show that η_s varies for the range of calculated P_s by about $\pm 0.03\%$ which we consider acceptable given the numerical precision used and the discretization of the distributions.) Also τ_r for the two signal photon energies differ, but the generation rate of excess quasiparticles depends on $h\nu_s$, as does the fraction of power lost before the quasistatic driven distributions are created. We would note that Eq. 5 correctly takes into account these underlying changes in τ_r due to signal and probe.

Fig. 7 shows that the distribution-averaged $\tau_{pb} \sim \tau_0^\phi$, which would often be assumed, but moreover $\tau_{pb} < \tau_0^\phi$. For $T/T_c = 0.1$, $\tau_{pb}(\Omega) \leq \tau_{pb}(2\Delta)$. $\tau_{pb}(\Omega)$ scales approximately as $1/\Omega$ in thermal equilibrium,¹⁰ hence the slight

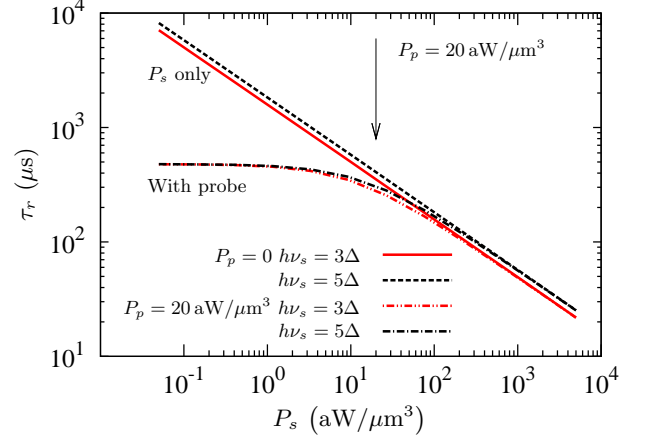


FIG. 6: (Color online) Distribution-averaged recombination times associated with the calculations of η_s shown in Fig. 5: (red) solid and double-dot dashed lines $h\nu_s = 3\Delta$, (black) dashed and dot-dashed lines $h\nu_s = 5\Delta$ with the values of P_p as indicated.

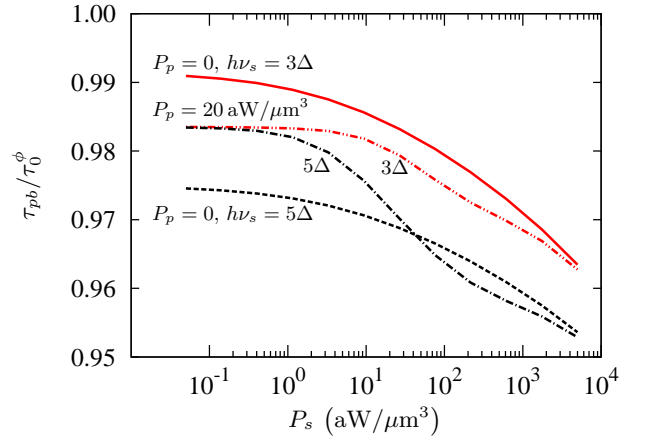


FIG. 7: (Color online) Distribution-averaged pair-breaking times used in the calculations of η_s shown in Fig. 5: (red) solid and double-dot dashed lines $h\nu_s = 3\Delta$, (black) dashed and dot-dashed lines $h\nu_s = 5\Delta$ with the values of P_p indicated.

reduction when τ_{pb} is calculated for the non-equilibrium distributions. We find that the variation of τ_{pb} as a function of the drive (both probe and signal) arises from the detailed spectra of the 2Δ -phonons for each case and is (to first-order) independent of the quasiparticle spectrum. It is possible to define an effective phonon temperature $T_{2\Delta}^{\text{eff}}$ that accounts for the total number of 2Δ -phonons. This approach accounts for the calculated τ_{pb} to within 1%, but not for the detailed behavior as a function of P_s . In the presence of the probe and signal the probe determines τ_{pb} if $P_p \gg P_s$ and in this case we find $T_{2\Delta}^{\text{eff}}$ more closely accounts for the calculated τ_{pb} . We would emphasize here that the full calculation of τ_{pb} is

necessary to find that η_s is independent of power P_s .

V. DISCUSSION AND CONCLUSIONS

We have presented calculations of the quasiparticle generation efficiency η_s for a pair-breaking signal in thin Al films at $T/T_c = 0.1$ with photon energies in the range $2\Delta \leq h\nu_s \leq 10\Delta$, $90 \leq \nu_s \leq 450$ GHz. We have also investigated the effect of including a probe with power and frequency typical of those used in low-noise KID read-out. The calculated detailed spectra show the effects of multiple interactions of the probe and the signal in the driven $f(E)$ with structure for example at $E = h(\nu_s + \nu_p)$. Our results demonstrate the importance of phonon loss on the quasiparticle creation efficiency. For thick films, $\tau_l/\tau_0^\phi = 8$, our calculations are in general agreement with earlier work for much higher signal energies, in calculations that ignore 2Δ -phonon loss, showing $\eta_s \simeq 0.59$. For resonators, thinner films would tend to be used since these maximize the kinetic inductance fraction of the response,¹ but these have reduced creation efficiencies by as much as 40% for the thinnest films considered here. Our calculations establish limits on the detection sensitivity of thin-film superconductors. The limiting Noise Equivalent Power of a thin-film detector is determined by generation-recombination noise^{6,24,27} and is given by $NEP = 2\Delta\sqrt{NV/\tau_r^{\text{eff}}}/\eta$ where V is the volume of the film and η the overall detection efficiency. η is the product of all detection efficiencies (including coupling efficiency) but η_s shown in Fig. 4 determines the limiting

efficiency in the thin-film case. Fig. [8] of Ref. 6 shows calculations of the limiting coupled NEP for $\eta = 0.59$ and 1 as a function of absorbed probe power. The present work shows that the best-possible coupled $NEPs$ are even higher than the case $\eta = 0.59$ shown there for much of the mm- and sub-mm spectrum in thin superconducting films. In deriving Eq. 5 we assumed that all quasiparticles have energy Δ . It is possible to take account of the energy distribution of the excess quasiparticles in the derivation and this would increase our calculated η_s by about 4%, but for consistency with earlier work we have assumed $E = \Delta$ for all of the excess.

We identify a coupling between the signal and probe that enhances η_s by about 2%. This maybe the effect described by Gulian and van Vechten,²⁸ who suggested that for low P_s multiple probe photon absorption by the higher energy primary peak of Fig. 2 (inset) occurs and some fraction of these quasiparticles are driven to energies $E \geq 3\Delta$. By contrast Fig. 2 suggests that 2Δ -phonon reabsorption occurs to enhance η_s . As the signal power increases there is a slight *reduction* in η_s because the relevant quantity is the fraction of quasiparticles in the photon peak driven above the pair-breaking threshold. The fraction reduces because the probe power is fixed and the probe generates (most of) the excess 2Δ -phonons. In future work we intend to extend the work to consider other low temperature superconductors, to investigate the detection linearity of a resonator with the driven distributions and also to consider the probe power levels that optimize detector $NEPs$.

* Electronic address: d.j.goldie@mrao.cam.ac.uk

¹ J. Zmuidzinas. Superconducting Microresonators: Physics and Applications. *Ann. Rev. Condens. Matter Phys.*, 3:169–214, 2012.

² J. J. A. Baselmans. Kinetic Inductance Detectors. *J. Low Temp. Phys.*, 167:292–304, 2011.

³ S. Friedrich. Superconducting tunnel junction photon detectors: Theory and applications. *J. Low Temp. Phys.*, 151:277–286, 2008.

⁴ G. N. Gol'tsman, O. Okunev, G. Chulkova, A. Lipatov, A. Semenov, K. Smirnov, B. Voronov, A. Dzardanov, C. Williams, and R. Sobolewski. Picosecond superconducting single-photon optical detector. *Appl. Phys. Lett.*, 79:705–707, 2001.

⁵ J. Bueno, M. D. Shaw, P. K. Day, and P. M. Echternach. Proof of concept of the quantum capacitance detector. *Appl. Phys. Lett.*, 96:103503, 2010.

⁶ D. J. Goldie and S. Withington. Non-equilibrium superconductivity in quantum-sensing superconducting resonators. *Supercond. Sci. and Tech.*, 26:015004, 2013.

⁷ P. J. de Visser, D. J. Goldie, P. Diener, S. Withington, J. J. A. Baselmans, and T. M. Klapwijk. Nonlinear electrodynamics of a superconductor due to the redistribution of quasiparticles. *Submitted to Phys. Rev. Lett.*, 2013, arXiv:cond-mat/1306.4992.

⁸ A. G. Kozorezov, A. F. Volkov, J. K. Wigmore, A. Peacock, A. Poelaert, and R. den Hartog. Quasiparticle-phonon downconversion in nonequilibrium superconductors. *Phys. Rev. B*, 61:11807–11819, 2000.

⁹ A. G. Kozorezov. Energy Down-Conversion and Thermalization in Metal Absorbers. *J. Low Temp. Phys.*, 167:473–484, 2012.

¹⁰ S. B. Kaplan, C. C. Chi, D. N. Langenberg, J. J. Chang, S. Jafarey, and D. J. Scalapino. Quasiparticle and phonon lifetimes in superconductors. *Phys. Rev. B*, 14:4854–4873, 1976.

¹¹ S. B. Kaplan. Acoustic matching of superconducting films to substrates. *J. Low Temp. Phys.*, 37:343–365, 1979.

¹² J. J. Quinn and R. A. Ferrell. Electron Self-Energy Approach to Correlation in a Degenerate Electron Gas. *Phys. Rev.*, 112:812–827, 1958.

¹³ E. M. Gershenzon, G. N. Gol'tsman, V. D. Potapov, and A. V. Sergeev. Restriction of microwave enhancement of superconductivity in impure superconductors due to electron-electron interaction. *Solid State Commun.*, 75:639–641, 1990.

¹⁴ B. L. Altshuler and A. G. Aronov. Electron-Electron Interactions in Disordered Systems. In A. L. Efros and M. Pollak, editors, *Modern Problems in Condensed Matter Physics*, page 1. North-Holland, Amsterdam, 1985.

- ¹⁵ A. V. Sergeev and M. Y. Reizer. Photoresponse Mechanisms of Thin Superconducting Films and Superconducting Detectors. *Int. J. Mod. Phys.*, 10:635–667, 1996.
- ¹⁶ N. Rando, A. Peacock, A. van Dordrecht, C. Foden, R. Engelhardt, B. G. Taylor, P. Gare, J. Lumley, and C. Pereira. The properties of niobium superconducting tunnel junctions as X-ray detectors. *Nucl. Instrum. Methods*, A313:173–195, 1992.
- ¹⁷ M. Kurakado. Possibility of high resolution detectors using superconducting tunnel junctions. *Nucl. Instrum. Methods*, 196:275–277, 1982.
- ¹⁸ R. A. Hijmering, P. Verhoeve, D. D. E. Martin, A. G. Kozorezov, J. K. Wigmore, R. Venn, P. J. Groot, and I. Jerjen. Efficiency of quasiparticle creation in proximized superconducting photon detectors. *J. Appl. Phys.*, 105:123906, 2009.
- ¹⁹ A. Zehnder. Response of superconducting films to localized energy deposition. *Phys. Rev. B*, 52:12858–12866, 1995.
- ²⁰ J. J. Chang and D. J. Scalapino. Nonequilibrium superconductivity. *J. Low Temp. Phys.*, 31:1–32, 1978.
- ²¹ G. M. Eliashberg. Inelastic Electron Collisions and Nonequilibrium Stationary States in Superconductors. *Sov. Phys. JETP*, 34:668–676, 1972.
- ²² P. J. de Visser, J. J. A. Baselmans, P. Diener, S. J. C. Yates, A. Endo, and T. M. Klapwijk. Number fluctuations of Sparse Quasiparticles in a Superconductor. *Phys. Rev. Lett.*, 106:167004, 2011.
- ²³ C. C. Chi and J. Clarke. Quasiparticle branch mixing rates in superconducting aluminium. *Phys. Rev. B*, 19:4495–4508, 1979.
- ²⁴ C. M. Wilson and D. E. Prober. Quasiparticle number fluctuations in superconductors. *Phys. Rev. B*, 69:094524, 2004.
- ²⁵ A. Rothwarf and B. N. Taylor. Measurement of recombination lifetimes in superconductors. *Phys. Rev. Lett.*, 19:27–30, 1967.
- ²⁶ J. J. Chang and D. J. Scalapino. Kinetic-equation approach to superconductivity. *Phys. Rev. B*, 15:2651–2670, 1977.
- ²⁷ P. J. de Visser, J. J. A. Baselmans, P. Diener, S. J. C. Yates, A. Endo, and T. M. Klapwijk. Generation Recombination Noise: The Fundamental Sensitivity Limit for Kinetic Inductance Detectors. *J. Low Temp. Phys.*, 167:335–340, 2012.
- ²⁸ A. M. Gulian and D. van Vechten. Nonequilibrium dynamic conductivity of superconductors: An exploitable basis for high-energy resolution detectors. *Appl. Phys. Lett.*, 67:2560–2562, 1995.